FABRICATION AND CHARACTERIZATION OF NANOPOROUS ENERGETIC SILICON

W. Churaman*, L. Currano, and M. Dubey
U.S. Army Research Laboratory
Adephi, MD, 20783-1197

C. Becker
University of Colorado at Boulder
Boulder, CO, 80309-0552

ABSTRACT

Arising as a new class of energetic material, nanoporous energetic silicon holds great potential for applications such as fuzing and thrust generation, which require large power output. In this paper we address fabrication and material characterization as well as monolithic integration of a hotwire initiator and packaging; the first steps toward a fully integrated MEMS/IC/energetic material system.

1. INTRODUCTION

Nanoporous energetic silicon is a new nanoenergetic material based on bulk silicon that offers great promise for on-chip integration of energetic materials. When nanoporous silicon is infused with any of a number of solid oxidizers, including perchlorates, nitrates, or molten sulfur, the mixture becomes highly energetic. The resulting nanoenergetic material can be ignited via friction, heat, or focused white light (Clement et al., 2005). The porosity, pore size, and internal surface area of the pores allow for a degree of control over the energetic properties. If the integration challenges can be resolved, the existing silicon IC and MEMS infrastructure can be leveraged for a new class of devices that exploit the high energy density and extremely fast energy release rate of nanoenergetic materials

2. FABRICATION

Our nanoporous silicon is created via an electrochemical etch in a 1:1 mixture of 49% HF and ethanol. Ethanol is used in the electrolyte solution because of the hydrophobic and organophillic characteristic of the nanoporous silicon. It removes the hydrogen bubbles on the surface of the silicon wafer during the etch, serving as a surfactant agent (Arrand, 1997). We begin with a <100> oriented, p-type boron doped silicon wafer with 1-30 ohm-cm resistivity. Prior to the etch, a Ti/Pt layer of metal is deposited on the backside of the wafer to evenly distribute the electrical potential across the wafer. The wafer is then annealed at 700°C for 60 seconds to reduce the contact resistance between the Ti/Pt and the silicon. A gold wire suspended in the HF:ethanol solution above the top of the sample serves as the cathode during the etch. During the electrochemical etch the fluorine atoms attack the underlying Si-Si bonds and release silicon in the form of two gaseous desorption products – a free radical, SiF_2, and the stable product SiF_4 (Flamm, 1990). The radical species then combine with more fluorine to form the stable SiF_4. The pores etch preferentially in the <100> direction due to the increased probability of enhanced nucleation sites that result from the nucleation of current bursts generated during the electrochemical etch (Carstensen et al., 2000)). When the etch is stopped, the nanoporous surface remains hydrogen passivated.

The electrochemical etch parameters determine the structural properties of the porous silicon. Variation of the etch current density, etch time, concentration of the electrolyte, and the doping and resistivity levels of the bulk silicon result in changes to the porosity and pore structure of the silicon material (Clement et al., 2004). Our standard electrochemical etch procedure uses a current density of $20mA/cm^2$ for a period of 30 minutes, resulting in a nanoporous Si layer that is ~35μm deep with pore diameters around 3.5nm. This recipe was chosen primarily for mechanical stability of the porous silicon layer, so that a hotwire initiator can be deposited on top without cracking the porous silicon. Figure 1 shows a top-down TEM view of a nanoporous silicon sample that has been etched using our standard recipe.

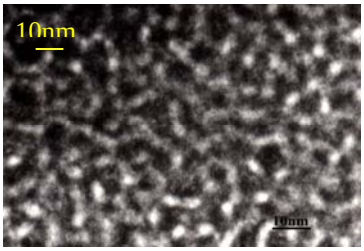

Figure 1 TEM of nanoporous Si

3. POROUS STRUCTURE CHARACTERIZATION

To begin to understand the reactive nature of the nanoporous silicon when combined with an oxidizer, we

Report Documentation Page

Form Approved
OMB No. 0704-0188

1. REPORT DATE	2. REPORT TYPE	3. DATES COVERED
DEC 2008	**N/A**	**-**

4. TITLE AND SUBTITLE	5a. CONTRACT NUMBER
Fabrication And Characterization Of Nanoporous Energetic Silicon	5b. GRANT NUMBER
	5c. PROGRAM ELEMENT NUMBER
6. AUTHOR(S)	5d. PROJECT NUMBER
	5e. TASK NUMBER
	5f. WORK UNIT NUMBER
7. PERFORMING ORGANIZATION NAME(S) AND ADDRESS(ES) **U.S. Army Research Laboratory Adephi, MD, 20783-1197**	8. PERFORMING ORGANIZATION REPORT NUMBER
9. SPONSORING/MONITORING AGENCY NAME(S) AND ADDRESS(ES)	10. SPONSOR/MONITOR'S ACRONYM(S)
	11. SPONSOR/MONITOR'S REPORT NUMBER(S)

12. DISTRIBUTION/AVAILABILITY STATEMENT
Approved for public release, distribution unlimited

13. SUPPLEMENTARY NOTES
See also ADM002187. Proceedings of the Army Science Conference (26th) Held in Orlando, Florida on 1-4 December 2008, The original document contains color images.

14. ABSTRACT

15. SUBJECT TERMS

16. SECURITY CLASSIFICATION OF:			17. LIMITATION OF ABSTRACT	18. NUMBER OF PAGES	19a. NAME OF RESPONSIBLE PERSON
a. REPORT	b. ABSTRACT	c. THIS PAGE			
unclassified	**unclassified**	**unclassified**	**UU**	**6**	

characterized the physical properties of our nanoporous structure. Nanoporous silicon is characterized by the porosity, pore size, and thickness of the nanoporous layer. The porosity is the fraction of void within the porous layer (Halimaoui, 1997). The accepted convention for determining the porosity of the nanoporous Si is based on a gravimetric technique (Halimaoui, 1997), which involves first weighting the sample prior to the anodisation (m_1), weighing after the anodisation (m_2), and finally after removal of the entire porous layer (m_3). The porosity is given by Eq. 1. The thickness (W) of the etched porous layer can be calculated using Eq. 2, where S is the area of the wafer exposed to HF during anodisation and d is the density of the bulk silicon. Alternatively, the thickness of the layer can be measured by cleaving the sample in half and imaging the cross-section of the porous layer in an SEM.

$$P(\%) = \frac{(m_1 - m_2)}{(m_1 - m_3)} \quad (1)$$

$$W = \frac{(m_1 - m_3)}{S * d} \quad (2)$$

The porosity is highly dependent on the HF concentration and current density (mA/cm^2), where the HF is mixed with ethanol to increase the homogeneity of the porous silicon layer (Halimaoui, 1997). Figure 2 shows the porosity measured gravimetrically and its dependence on the HF concentration. The 25% concentration solution here refers to a 1:1 volumetric mixture of 49% HF and ethanol, and the 33% concentration corresponds to a 2:1 mixture of 49%HF and ethanol. The porosity can be seen to increase with increasing current density and decrease with increasing HF concentration. Both of these trends are supported by existing porous silicon literature (Halimaoui, 1997). With a 25% HF/EtOH solution, the porosity can be well above 50% at a relatively low etch current of 5mA/cm^2.

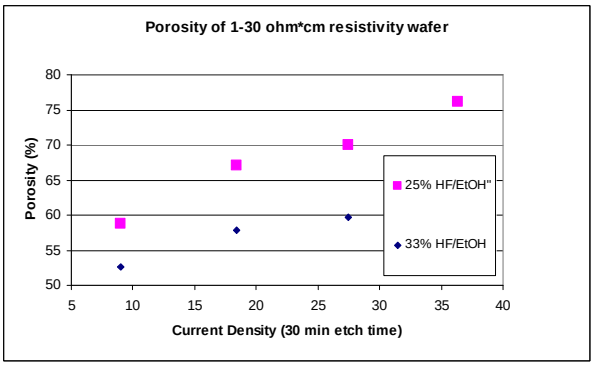

Figure 2 Gravimetric analysis of the porosity as a function of HF/EtOH concentration

Characterization of the pore diameter and surface area is based on gas adsorption analysis of the porous layer after the pores are etched. Figure 3 shows the pore diameter as a function of solution concentration and current density for the same etch time of 30 minutes. The adsorption data indicates that the pore diameter increases with decreasing HF concentration of the HF:ethanol solution. The 25% HF/EtOH solution results in larger pore diameter in comparison to 33% HF/EtOH solution. The pore diameter is 8-10Å larger in samples etched with the 25% HF/EtOH electrolyte. The pore size also increases with increasing current density. Again, these trends are expected based on the existing literature (Halimaoui, 1997).

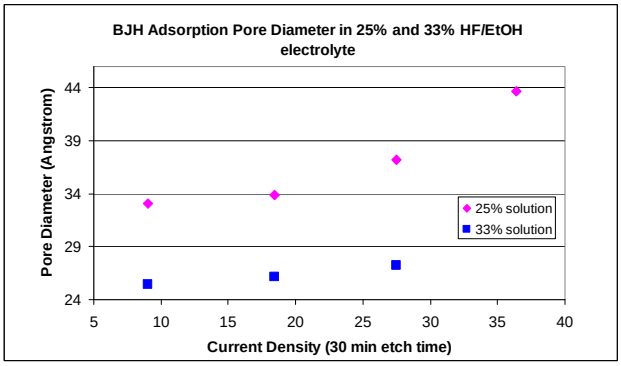

Figure 3 BET volumetric analysis of the pore diameter varying the HF/EtOH concentration

4. OXIDIZER MIGRATION

Among the most popular oxidizers, calcium perchlorate and sodium perchlorate have shown the most promise in terms of their ability to stay inside the porous network. The success of the reaction also depends on the time it takes to heat the nanoporous Si layer. It has been shown that below a certain heating ramp, the oxidizer decomposes before it is able to react with the silicon fuel, causing the reaction to fail (Clement et al., 2004). Several factors contribute to the ability of the oxidizer to successfully interact with the nanoporous layer, some of which include their solubility and hygroscopic or hydroscopic nature. $NaClO_4$ is the preferred choice of oxidizer because it contains only one crystal water and is not as hygroscopic as some of the other perchlorates (Clement et al., 2004). A major challenge that exists in the oxidization process involves maintaining the strength of the reaction by ensuring that the oxidizer remains inside the pores. The strength of the reaction is reduced due to the oxidizer migrating out of the pores. Once the oxidizer has been applied to the samples, the samples are placed in a dry box allowing the $NaClO_4$ to dry inside the pores. Over time, the $NaClO_4$ appears to creep out of the porous network. Figure 4 shows a sample oxidized with a 2.4M solution of $NaClO_4$ dissolved in methanol where the

salt crystals have migrated out of the pores after being dried for 15 minutes. Test samples, etched and dried under similar conditions did not exhibit the same oxidizer migration when oxidized with 1.6M in methanol.

Figure 4 Sample oxidized with 2.4M $NaClO_4$ in methanol showing migration of salt out of the pores.

An additional test was carried out to determine the effect of drying a sample etched at a current density of 20mA/cm^2. The oxidizer $NaClO_4$ was mixed in anhydrous ethanol. The mass of the sample was taken immediately after application of oxidizer, which weighted 0.489g. After initially drying the sample in an N_2 dry box for 2 minutes, a mass of 0.483g was measured. The sample was dried for 30 additional minutes, but did not exhibit significant variation in mass. After three days in a dry environment, little of the salt had migrated out of the pores, and the mass remained constant. It appears that the migration of the oxidizer may be dependent on the content of water molecules inside the nanoporous structure. Using anhydrous ethanol versus methanol to dissolve the salt minimizes the water content in the pores. Due to the larger concentration of water in the methanol, the drying process appears to be causing the dislocation of the salt as the water inside the porous network begins to evaporate. This process pushes the salt crystals out of the pores. Further investigation needs to be done to determine the water content inside the pores to better correlate the amount of water evaporated with variation in sample mass as a result of drying.

5. RESULTS AND DISCUSSION

As mentioned above, the etch recipe for our porous silicon fabrication was chosen for mechanical stability of the porous layer. Due to removal of some silicon atoms from the lattice, there is an inherent tensile stress in the porous silicon network. The mechanical stability of the porous layer is compromised when the stress exceeds the fracture strength of silicon. This can easily occur as the pore walls are very thin and have many stress concentrations due to roughness and branching of the pores. As the porosity and pore size increases with increasing etch current density or decreasing HF concentration, the mechanical stability decreases and the porous silicon becomes prone to cracking. The cracking often worsens due to surface tension induced stresses when the porous silicon is dried, even when the etch solution is replaced with a low surface tension fluid such as pentane. The cracking further worsens when the hotwire is deposited due to the residual stress in the metal. Finally, the cracking worsens one more time when the oxidizer is deposited and the solvent evaporates. Selecting a current density which does not result in cracking of the porous layer even after all of these exacerbating steps required limiting the current density to <20mA/cm^2. There is a significant tradeoff here, as higher porosity and larger pore sizes appear to correlate in our experiments with louder and brighter reactions (i.e. more or faster energy release). These are qualitative observations; the dependencies have not yet been quantitatively studied, but there is definitely some dependency. The variables are complex, especially since the precise filling factor of the pores with the oxidizer is unknown.

6. HOTWIRE DESIGN AND TEST

The exothermic reaction of porous silicon when combined with an oxidizer is initiated by heat generated in the hotwire. The transfer of heat between the hotwire and the nanoporous Si is assumed to take place through the Si nanocrystallites rather than through the individual pores (Lysenko et al., 2000). Based on this assumption, the thermal conductivity of the prepared nanoporous silicon can be described in Eq. 3 (Lysenko et al., 2000) where k_{eff} is the effective thermal conductivity of an individual Si nanocrystallite, P is the layer porosity, and g_o is the percolation strength, which is identified as the fraction of the solid phase contributing the heat conduction as a result of the crystal interconnects.

$$k_{nano-PS} = k^{cr}{}_{eff}\ (1-P)g_o \tag{3}$$

The thermal conductivity of our porous silicon as predicted by this equation is 0.137 $Wm^{-1}K^{-1}$ for a sample etched at 30mA/cm^2 in 25% HF in EtOH for 30 minutes. The porosity of the etched sample is 70%. This is 3 orders of magnitude below that for solid silicon, and this allows the hotwire to reach far higher temperatures with the same amount of joule heat generation. So the hotwire initiator actually operates far more efficiently because it is on porous silicon.

The interaction that occurs at the interface of the nanoporous Si and the hotwire allows for thermal ignition to take place. Hotplate initiation tests indicate that an ignition temperature of 225°C is necessary to trigger the exothermic reaction of a 40μm porous layer oxidized with a 3.2M solution of sodium perchlorate. The finite element hotwire model in Figure 5 was developed to determine the achievable temperatures based on the geometric design of the hotwire. The design is based on a bow-tie geometry,

where the center of the hotwire is narrowed in order to obtain large localized heating of the hotwire.

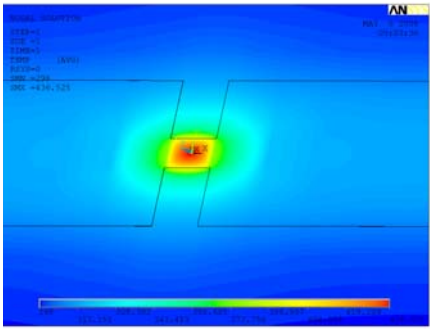

Figure 5 ANSYS finite element model showing hotwires ability to achieve localized heating up to 250°C

The finite element ANSYS model was simulated by applying a fixed voltage across the hotwire structure to determine the thermal response and localization of heat in the system. The model does not take into consideration the interface between the hotwire and the nanoporous silicon layer. Figure 6 shows a comparative analysis that was performed by varying the width of the center region of the hotwire from 400μm to 300μm, and using a FLIR camera to monitor the temperature of the hotwire while ramping up the applied voltage across the wire. At an applied voltage of 13V, the results indicate that narrowing the center of the hotwire leads to a 160°C increase in the achievable temperature. The hotwires were deposited on unetched bulk silicon for the FLIR tests to avoid ignition of the nanoporous Si, and potential damage to the camera objectives. Therefore the expected temperature at a given voltage should be much higher than that reflected in Figure 6.

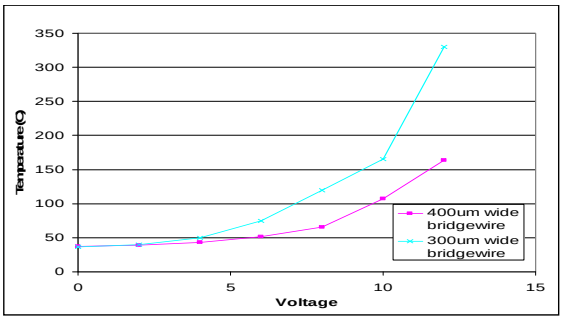

Figure 6 Dependence of achievable temperature as a function the width of the hotwire

Additional FLIR tests were performed to determine the thermal characteristics of potential hotwire metals, with the goal being to achieve high localized heating of the hotwire above the initiation temperature of 225°C for the nanoporous Si, with electrical resistance < 10ohms. In order to reduce the resistivity of the hotwire, Pt and Au were chosen as two potential hotwire metals. The Au hotwire, although having extremely good electrical properties, failed at fairly low temperature because the Au molecules were rapidly diffusing through the Ti adhesion layer and reacting with the silicon substrate, resulting in a rapid increase in resistance of the electrical current path. The Pt required higher voltages in order to reach the ignition temperatures. Because the low resistivity of Au allows for low voltage initiation, we now use a 200/1000/3800Å Ti/Pt/Au hotwire stack. The Pt serves as an effective diffusion barrier for the gold, allowing the hotwire to handle currents as large as 1A without failing.

A shadow masking technique has been developed to deposit the hotwire material directly on top of the nanoporous Si. A Si shadow mask is fabricated on a 4 inch bulk silicon wafer. The geometric dimensions of the hotwire are photolithographically patterned on the wafer and a through wafer DRIE transfers the features to the wafer. The shadowmask is aligned to the nanoporous silicon wafer under a microscope, taped in place, and the hotwire metals are evaporated through the mask. Figure 7 shows an optical image of a hotwire that has been shadow masked directly onto a layer of nanoporous Si. The halo effect around the hotwire is due to bleed-out of the metal during the deposition arising from imperfect contact with the shadowmask. The resistance of the hotwire is not easily controlled primarily because of the surface roughness of the sample and the bleedout.

Figure 7 Optical image of the hotwire monolithically integrated on porous Si

In addition to characterizing the thermal properties of the hotwire, FLIR tests were done to analyze the exothermic reaction of the oxidized nanoporous energetic silicon with the integrated hotwire. A $1cm^2$ sample oxidized with gadolinium nitrate $Gd(NO_3)_3$was mounted perpendicular to the FLIR camera, where the plume of hot gases ejected from the sample would appear in the field of view. Figure 8 shows a plume of ejected gas that reaches 460°C at an ignition temperature of 225°C.

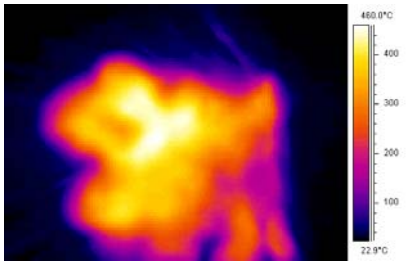

Figure 8 FLIR test of achievable reaction temperature (FLIR Measurement of NXS reaction)

6. PACKAGING

Once the hotwire has been successfully deposited on the nanoporous Si, the chip is then placed in an electronics package. The two ends of the hotwire are wirebonded to two pinouts on the package, and the oxidizer is then applied to the nanoporous material. This allows electrical connection to the hotwire unimpeded by oxidizer contamination on top of the hotwire, and avoids exposure of the active energetic material to heat during the wirebonding. Bonds can not be made to the portion of the hotwire directly on top of the nanoporous silicon because its lack of structural stability causes the hotwire to peel up if a wirebond is attempted here.

The exothermic reaction can then be initiated by applying a voltage across the hotwire to generate joule heating. Figure 9 below shows a packaged nanoporous silicon energetic device with $NaClO_4$ oxidizer on it. The 300μm long hotwire for this device is a sputtered Ti/Pt layer, with a center section that is narrowed to 50μm. The dark brown circular region is a ~1cm^2 area of nanoporous silicon, and the white crystalline material is the oxidizer ($NaClO_4$) that has been applied to the nanopores using an eye dropper, which can result in excess salt crystals on the bulk silicon.

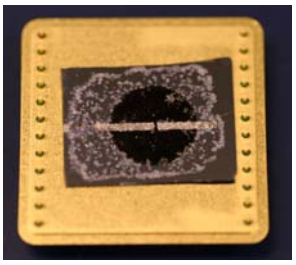

Figure 9 Packaged nanoporous silicon device

7. SENSITIVITY

We have conducted a series to tests to understand and quantify the sensitivity of the energetic nanoporous silicon to shock. The chips were mounted to the test platform on a linear shock machine in order to test their response to controlled shock levels. Progressively higher half-sine shocks were applied to the device, beginning with 53g for 10ms. The samples did not ignite spontaneously even up to a limit of 5131g with a duration of 0.2ms. Figure 10 shows the accelerometer output from the shock test at 5131g at duration of 0.2ms. Upon completion of the shock testing, the samples where set off using friction from a diamond scribe to ensure that we were not running the experiments with 'duds'.

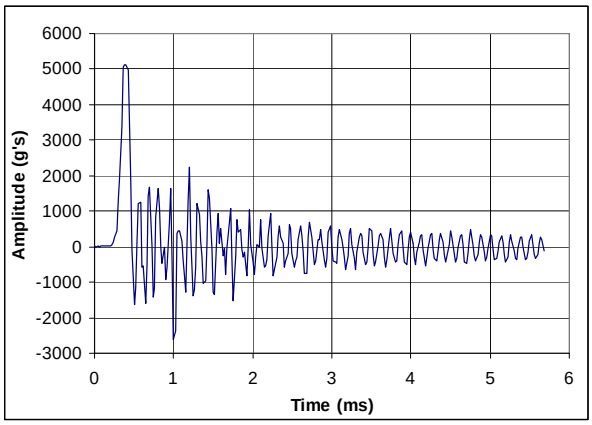

Figure 10 Packaged nanoporous silicon device

Although limited by the upper bound of the shock table capability, the samples were never triggered by any of the shock events, indicating a low sensitivity to shock. This is promising for the potential use of nanoporous energetic silicon in projectiles. Further tests must be done at higher shock levels to determine the actual upper bound at which a shock event may trigger a potential reaction of the oxidized nanoporous silicon.

CONCLUSIONS

Nanoporous energetic silicon holds great potential for on-chip integration of energetic materials. We have demonstrated the ability to control the nanoporous structure through the fabrication process by controlling the etch parameters. Based on the etch conditions we have been able to demonstrate variability in porosity, surface area, and pore diameter. A strong dependence of energetic properties such as reaction propagation velocity on the mechanical properties of the porous silicon is definitely observed, although it is still not well understood or characterized. We have also demonstrated the monolithic integration of a hotwire initiator, wirebonding into an electronics package and ignition with the application of a current on the order of several hundred milliamps. While far more work remains, this new class of energetic offers great versatility in terms of application and potential system integration.

ACKNOWLEDGEMENTS

The authors would like to acknowledge Mr. Mark Gelak of the Armaments Research Development and Engineering Command (ARDEC) for continued funding and support of the ongoing work that has gone into developing nanoporous silicon energetics and for the collaborative exchange of knowledge and guidance.

REFERENCES

Arrand, H., 1997: Optical Wavguides and Components Based on Porous Silicon, *The University of Nottingham George Green Institute Ph.D Theses*, 3-11.

Carstensen, J., Christophersen, M., and Foll, H., 2000: Pore Formation Mechanisms for the Si-HF System, *Materials Science and Engineering: B*, **Vol. 69-70**, 23-28.

Clement, D., Diener, J., and Kovalev, D., 2004:. Explosive Porous Silicon – From Laboratory Accident to Industrial Application, *Proceedings of the 35th International Conference of ICT*, **5-1**.

Clement, D., Kiener, J., Gross, E., Kunzner, N., Timoshenko, V., and Kovalev, D., 2005: Highly explosive nanosilicon-based composite materials, *Physica Status Solidi*, **(a) 202, No. 8**, 1357-1364.

Flamm, D., 1990: Mechanisms of silicon etching in fluorine- and chlorine-containing plasmas, *Pure and Appl. Chemistry*, **Vol. 62, No. 9**, 1709-1720.

Halimaoui, A., 1997: Porous silicon formation by anodisation, *Properties of Porous Silicon: emis Datareviews Series* **No. 18**, 12-23

Lysenko, V., Roussel, PH., Remaki, B., Delhomme, G., Dittmar A., and Barbier, D., 2000:, Study of Nano-Porous Silicon with Low Thermal Conductivity as Thermal Insulating Material *Journal of Porous Materials*, **7**, 177-182.